JACS
JOURNAL OF THE AMERICAN CHEMICAL SOCIETY
Communication
pubs.acs.org/JACS

Intermediate-Range Structure of Self-Assembled Cobalt-Based Oxygen-Evolving Catalyst

Christopher L. Farrow,[†] D. Kwabena Bediako,[‡] Yogesh Surendranath,[‡] Daniel G. Nocera,*[,‡] and Simon J. L. Billinge*[,†,§]

[†]Department of Applied Physics and Applied Mathematics, Columbia University, New York, New York 10027, United States
[‡]Department of Chemistry and Chemical Biology, Harvard University, Cambridge, Massachusetts 02138, United States
[§]Condensed Matter Physics and Materials Science Department, Brookhaven National Laboratory, Upton, New York 11973, United States

Supporting Information

ABSTRACT: Continual improvements in solar-to-fuels catalysis require a genuine understanding of catalyst structure−function relationships, not only with respect to local order, but also intermediate-range structure. We report the X-ray pair distribution function analysis of the nanoscale order of an oxidic cobalt-based water-splitting catalyst and uncover an electrolyte dependence in the intermediate-range structure of catalyst films. Whereas catalyst films formed in borate electrolyte (CoB_i) exhibit coherent domains consisting of 3−4 nm cobaltate clusters with up to three layers, films deposited in phosphate electrolyte (CoP_i) comprise significantly smaller clusters that are not coherently stacked. These structural insights are correlated with marked differences in activity between CoP_i and CoB_i films.

Hydrogen and oxygen generation by solar-driven water splitting provides a means to store sunlight in a renewable manner.[1−3] However, the kinetic complexity of water splitting,[4] particularly for the oxygen evolution reaction (OER), mandates the use of catalysts to store and discharge the redox equivalents productively by performing the $4e^- - 4H^+$ proton-coupled electron transfer (PCET) of the OER at low overpotential.[5−11] Electrodeposited thin-film OER catalysts, which self-assemble from solutions of $Co^{2+}(aq)$[12−14] and $Ni^{2+}(aq)$[15,16] in the presence of a buffering electrolyte, such as phosphate (P_i), methylphosphonate (MeP_i), or borate (B_i), perform the OER remarkably well.[17] Extended X-ray absorption fine structure (EXAFS) investigations[18−20] of these catalyst films establish that they are composed of edge-sharing MO_6 clusters of molecular dimensions. A recent X-ray scattering and PDF analysis study[21] has extended the initial EXAFS studies and demonstrated that the domains of CoP_i films consisted of clusters comprising on the order of 14 Co ions.

Whereas EXAFS provides key insight into the *local* order in these films, atomic pair distribution function (PDF) has the added benefit that it affords a direct probe that is also sensitive to *intermediate*-range structure on the nanoscale.[22−24] Nanoscale structure is a crucial determinant of the electronic structure of a variety of functional materials. In the case of the self-assembled OER catalysts, intermediate-range order in these porous thin films is also anticipated to be critical to charge/mass transport between active sites and hence overall catalytic activity. Indeed, changes in microstructure of thin films and electronic structure would be expected to impact the activity and performance of any OER anode. The kinetics of CoP_i nucleation and film deposition indicates that the electrolyte plays a pivotal role in modulating catalyst self-assembly.[25] We surmised that the identity of the electrolyte could impact the structure of Co-OEC, and in the future permit the tuning of catalytic activity. To this end, the self-assembled Co-P_i/B_i films offer a unique platform to explore nanoscale structure−activity relationships of OER catalysts at length scales beyond the molecular dimension. We now show by X-ray PDF analysis of CoP_i and CoB_i films that the B_i templates a unique intermediate layered microstructure, thus establishing the importance of film microstructure in overall catalytic activity.

Catalyst films were electrodeposited onto FTO plates (Hartford Glass) by controlled-potential electrolysis of $Co^{2+}(aq)$ solutions containing P_i or B_i at pH 7.0 or 9.2, respectively. Following electrodeposition, films were rinsed and dried in air, and catalyst material was removed from the substrate surface. Nanoparticulate (50 nm) Co_3O_4 was used as received (Sigma-Aldrich), and CoO(OH) was prepared according to an established procedure.[26] Samples were packed into polyimide capillary tubes for X-ray analysis. X-ray analysis was performed at the X7B beamline at the National Synchrotron Light Source (NSLS) at Brookhaven National Laboratory. Diffraction data were collected using the rapid acquisition pair distribution function (RaPDF) technique,[27] utilizing a 2D X-ray detector. Full experimental details pertaining to sample preparation and X-ray analysis are provided in the Supporting Information (SI).

All raw 2D data images were azimuthally integrated and converted to intensity versus 2θ using the software Fit2D,[28] where 2θ is the angle between the incident and scattered X-rays. The data were corrected using PDFgetX3,[29] a home-written data analysis program, to obtain the total scattering structure function, $S(Q)$, where Q is the magnitude of the scattering vector (as defined in the SI) and the PDF, $G(r)$. Plots of $Q(S(Q) - 1)$ for all samples are shown in Figure 1a, and $G(r)$ plots for CoP_i and CoB_i are shown in Figure 1b. PDFs of all samples are presented in Figure S1. Unlike the crystalline analogues which exhibit sharp

Received: February 4, 2013
Published: April 2, 2013

   dx.doi.org/10.1021/ja401276f | J. Am. Chem. Soc. 2013, 135, 6403−6406

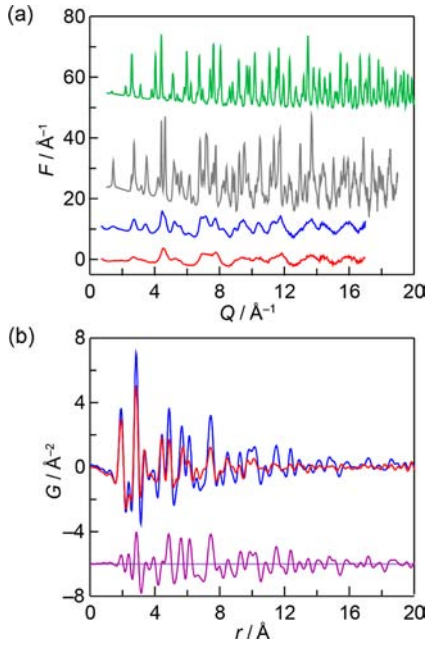

Figure 1. (a) Structure functions for (from top to bottom) crystalline Co_3O_4 (green line), CoO(OH) (grey line), and nanocrystalline samples of CoB_i (blue line) and CoP_i (red line). (b) Comparison of PDFs of CoB_i (blue line) and CoP_i (red line). PDFs have been truncated at $r = 20$ Å to highlight the differences. The difference is shown by the lower trace (purple line), which is offset for clarity.

Bragg peaks in the diffraction pattern (Figure 1a) and possess PDFs that extend to high r (Figure S1), the catalyst samples exhibit only diffuse scattering due to finite size effects (Figure 1a). However, PDFs of CoP_i and CoB_i display sharp peaks in real space (Figure 1b), indicating a well-defined local order (i.e., they are not glassy). The peaks diminish with increasing r, signifying that the samples are nanocrystalline with domain sizes between 15 and 30 Å. It is also evident from Figure 1b that CoB_i possesses more structural coherence than CoP_i, since there is a wider range of r for the former over which structural correlations persist. Whereas Du and co-workers have observed extra features in their PDF data that were attributed to CoO cube defects and distortions to the terminal Co−O positions,[21] we do not observe any evidence for such features. The fact that our samples are catalytically active without the presence of the defect features suggests that they are not essential for the activity, though additional studies are required to resolve this issue.

Two crystalline structural analogues, Co_3O_4 and CoO(OH), were also measured for structural comparison to the CoP_i/B_i samples. Their PDFs were truncated to simulate nanoparticle effects and compared to CoP_i and CoB_i (Figures S2−S5). In general, there is poorer agreement of CoP_i/B_i to Co_3O_4 (Figures S2 and S3) as compared to CoO(OH) (Figures S4 and S5), indicating that the CoP_i/B_i samples are of the cobaltate structure, in agreement with previous EXAFS and PDF structural studies.[18−21] However, there is significantly poorer agreement between CoO(OH) and the CoP_i/B_i at high r compared to low r, representing some difference in intermediate-range structure. For example, a significant discrepancy in peak position between CoO(OH) and either CoP_i and CoB_i is found in the doublet between 4 and 5 Å. The CoO(OH) structure consists of aligned layers of edge-shared CoO_6 octahedra with hydrogen atoms in the interlayer region.[30] The first peak in the doublet arises from the nearest-neighbor *inter*layer Co−Co distance in the CoO(OH) structure, and the second peak is from the second nearest-neighbor *intra*layer Co−Co distance. Since the largest discrepancy is in the position of the first peak of the doublet, this indicates that CoP_i and CoB_i have the CoO(OH) structure, but with diminished coherence in the stacking direction due to turbostratic disorder between stacked layers, or because the clusters are not coherently stacked at all.

Preliminary modeling was performed using the PDFgui software,[31] with the model PDFs attenuated by the characteristic function for a sphere. Modeling was performed according to standard procedures,[22,32] using the maximum number of parameters allowed by the space groups of the model structures. In agreement with our initial observations, the CoO(OH) model performed better by a considerable margin than Co_3O_4 (Figures S6 and S7), as evidenced by the greatly improved goodness-of-fit parameter, R_w. Both models refined with large cobalt atomic displacement parameters along the c-axis of the cell, providing evidence for turbostratic disorder among the stacked layers.[32,33]

More advanced modeling was performed using atomistic nanoparticle models created from the CoO(OH) structure. These models were fit using our recently developed SRREAL and SRFIT programs.[34] Models were created for refinement using a nanoparticle template approach; a geometric shape is used to excise a nanoparticulate model from a crystal structure. This allows us to vary not only the crystal structure, but also the dimensions of the nanoparticle by varying the template. It also allows us to decorate the model with additional scatterers and to distort the model. This was not done here, but will be explored in future modeling efforts. The nanoparticle models for CoB_i and CoP_i were created using a cylindrical template. The template was allowed variable dimensions and location, with the axis of the cylinder aligned with the c-axis of the CoO(OH) structure. For simplicity, hydrogen atoms were excluded from the models. Since circular cuts were made in the hexagonal layers, the resulting structures that were used for modeling did not necessarily have fully coordinated Co ions at the perimeter. The resulting finite-sized nanoparticle models are then used to calculate the PDF using the Debye equation. Unlike the PDFgui approach, this method does not use periodic boundary conditions.

The refined PDF fits and models for CoB_i and CoP_i catalysts are shown in Figures 2 and 3, and some structural parameters are tabulated in Table S1. The CoB_i model has three layers on average, and the diameter of the layers is approximately 35 Å. We

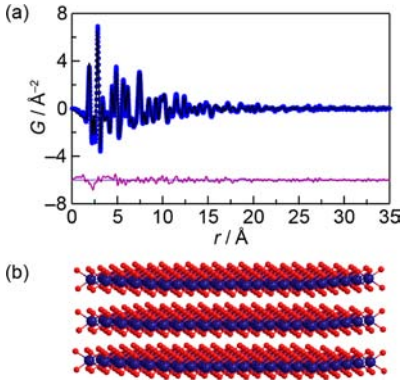

Figure 2. (a) Cylindrical atomistic model fit (black line) to the CoB_i catalyst PDF data (blue circles). The difference curve is shown in purple, and is offset for clarity. (b) View of the refined model for the average coherent domain in CoB_i films.

dx.doi.org/10.1021/ja401276f | J. Am. Chem. Soc. 2013, 135, 6403−6406

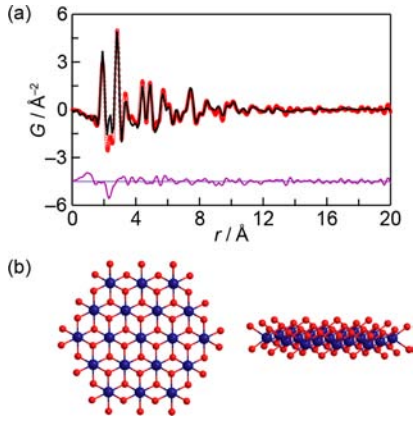

Figure 3. (a) Cylindrical atomistic model fit (black line) to the CoP_i catalyst PDF data (red circles). The difference curve is shown in purple, and is offset for clarity. (b) Two views of the refined model for the average coherent domain in CoP_i films.

attempted to constrain the model to a single layer, but this furnishes a poorer fit (Figure S8), suggesting that the coherent domains of CoB_i do indeed consist of multiple layers of clusters with weak, but significant interlayer correlations. Compared to the crystalline CoO(OH) compound, the *c*-axis is significantly larger (Table S1), which indicates an expansion of the layers, perhaps to accommodate species larger than protons in the interlayer region such as weakly scattering or disordered electrolyte ions, though these were not identified. The refined CoP_i model and fit (Figure 3) indicate that the diameter of the clusters is approximately 14 Å, considerably smaller than those of CoB_i. This model was given the flexibility to form layers, but did not. This suggests that unlike CoB_i, the coherent domains of the catalyst consist of single-layer clusters like those shown in Figure 3b whose arrangements are significantly disordered in the film.

The dependence of structure on deposition potential was evaluated for fixed electrolyte conditions. CoP_i films were deposited at 1.0−1.1 V vs NHE, and CoB_i films were deposited at 0.9−1.0 V vs NHE. No significant differences were observed over this range for films grown in P_i or B_i at varying potentials, indicating that it is the electrolyte, and not the potential, that directs these nanoscale structural changes in catalyst films.

Electrochemical data indicate that the intrinsic activity of CoB_i films is considerably better than that of CoP_i films as film thickness is increased. This is evident in Figure 4, where the geometric current density of the cobalt OER catalysts at a fixed overpotential of 400 mV is shown as a function of film loading. In

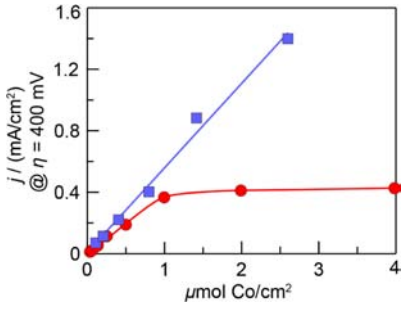

Figure 4. Stead-state current density, *j*, at an overpotential, η, of 400 mV for CoP_i (red circles) and CoB_i (blue squares) films with varying loading operated in KP_i pH 7.0 and KB_i pH 9.2 electrolyte, respectively. Lines are drawn simply as guides to the eye.

both cases, the performance of the anode can be improved by depositing thicker films. However, the behavior for CoB_i and CoP_i differs. Whereas the CoB_i films display a monotonic increase in activity with film thickness, the activity of CoP_i attains a limiting activity at catalyst loadings in excess of 1 μmol Co/cm^2. At loadings greater than 0.25 μmol Co/cm^2, CoB_i activity is significantly superior to that of CoP_i. These results suggest that the effective surface area of the CoB_i catalyst increases with increasing film thickness while preserving the intrinsic transport properties within the film. The PDF results now offer a concrete difference in CoP_i and CoB_i, thus allowing the first insight into a tangible structure−function correlation. The mesoscale ordering of the CoB_i film suggests enhanced catalytic activity. Electrochemical and stopped-flow spectroscopic studies using molecular model compounds establish that the mechanism for charge transport in these films is best thought of as involving a series of PCET self-exchange reactions between Co^{III} and Co^{IV} centers of different cluster subunits.[35] Along these lines, the larger domain size of CoB_i relative to CoP_i provides a mechanism to delocalize the mobile holes over a larger region, which can be manifest in more efficient charge transport owing to (1) fewer discrete hole hops needed in a given distance for charge transport among clusters and (2) a reduced reorganizational energy for electron transfer since charge is delocalized over a larger cluster area. Indeed, charge delocalization has been observed to enhance apparent self-exchange rates and attendant hole mobility on polymer[36,37] and nanoparticulate[38] films. In addition, interlayer hopping of holes may be facilitated by less disorder in a film comprising a multilayer CoB_i structure as compared to more disorder in the single-layer structure of CoP_i films. Together, these factors will contribute to an enhanced hole hopping rate, and hence a greater charge transport mobility in CoB_i films, accounting for the ability of these films to sustain higher net activity than CoP_i. In addition, we hypothesize that such nanoscale differences may impact a long-range morphology of these materials, such as their porosity and, by extension, their capacity for *mass* transport. Detailed transport and surface-area measurements will shed more light on these questions.

The electrolyte in OER self-assembly of Co and Ni/P_i and B_i films has several important roles. First, the anionic electrolyte is a mechanistic element of film nucleation and film growth. Second, the electrolyte is a proton acceptor in the PCET reaction of OER. Third, the electrolyte is the critical determinant of the self-healing nature of these films. The structural insights uncovered here by PDF analysis now indicate yet another important role of the electrolyte as an element that directs the intermediate-range structural order of the oxidic cobalt clusters within the films. Previous kinetic studies have provided a mechanistic framework for understanding the conflicting interactions between the buffering electrolyte as both proton acceptor and adsorbing anion.[25] Whereas the latter role inhibits catalyst assembly, the former serves to assist formation and growth of clusters by facilitating the PCET oxidation of Co^{2+} precursors.[25] Thus, it is reasonable to expect that the size of the domains formed would depend critically on the balance between these factors; a high binding constant between buffering anion and cobalt centers—most likely at the edges of nascent clusters—would favor the formation of new domains versus the growth of existing ones, whereas a weaker adsorption isotherm would promote larger domain sizes. The intercalation of anions between clusters, as observed in solid-state ^{31}P NMR studies of CoP_i,[39] may serve as a mechanism by which the electrolyte defines the degree of coherence in stacking of cobaltate clusters. The fundamental

dx.doi.org/10.1021/ja401276f | J. Am. Chem. Soc. 2013, 135, 6403−6406

thermodynamic and kinetic parameters that directly regulate catalyst size warrant further investigation, since electrochemical studies show that these nanoscale morphological changes have a marked impact on the activity with film thickness (Figure 4).

The CoP_i/B_i clusters are dimensionally reduced analogues of extended cobalt oxides. These PDF studies now show that this dimensional reduction extends beyond Co oxido cluster subunits, and in CoB_i a mesostructure is realized that captures the nascent layered structure of cobaltates such as $LiCoO_2$. In this regard, CoB_i provides a link between molecular and extended-solid OER catalysts. After nearly a century of research,[40,41] the mechanism of the OER at an atomistic level remains largely unknown for conventional transition metal oxides. Thus the CoB_i OER catalyst offers a molecular-like understanding of the structure–function relationships of OER oxide catalysts. The edges of the clusters are known to be especially important to OER activity in CoP_i and CoB_i films.[42−44] Hence, the results described herein suggest that traditional metal oxides may restructure to give metallate cluster active sites of the type observed in this study. Insights such as these, which provide a bridge between molecular and extended solids, should be useful to accelerating the discovery of both homogeneous and heterogeneous catalysts systems.

■ ASSOCIATED CONTENT

Supporting Information

Full experimental details, additional PDF data, and fitting plots. This material is available free of charge via the Internet at http://pubs.acs.org.

■ AUTHOR INFORMATION

Corresponding Author

dnocera@fas.harvard.edu; sb2896@columbia.edu

Notes

The authors declare no competing financial interest.

■ ACKNOWLEDGMENTS

X-ray experiments were carried out at the National Synchrotron Light Source, Brookhaven National Laboratory, which is supported by the DOE, Division of Materials Sciences and Division of Chemical Sciences, DE-AC02-98CH10886. Work in the Billinge group was supported by the DOE under DE-SC0001085. Work in the Nocera group was supported by Grant DE-SC0009565.

■ REFERENCES

(1) Cook, T. R.; Dogutan, D. K.; Reece, S. Y.; Surendranath, Y.; Teets, T. S.; Nocera, D. G. *Chem. Rev.* **2010**, *110*, 6474.
(2) Barber, J. *Chem. Soc. Rev.* **2009**, *38*, 185.
(3) Lewis, N. S.; Nocera, D. G. *Proc. Natl. Acad. Sci. U.S.A.* **2006**, *103*, 15729.
(4) Surendranath, Y.; Nocera, D. G. *Prog. Inorg. Chem.* **2011**, *57*, 505.
(5) Cukier, R. I.; Nocera, D. G. *Annu. Rev. Phys. Chem.* **1998**, *49*, 337.
(6) Eisenberg, R.; Gray, H. B. *Inorg. Chem.* **2008**, *47*, 1697.
(7) Betley, T. A.; Wu, Q.; Van Voorhis, T.; Nocera, D. G. *Inorg. Chem.* **2008**, *47*, 1849.
(8) Betley, T. A.; Surendranath, Y.; Childress, M. V.; Alliger, G. E.; Fu, R.; Cummins, C. C.; Nocera, D. G. *Philos. Trans. R. Soc. B* **2008**, *363*, 1293.
(9) Hammes-Schiffer, S. *Acc. Chem. Res.* **2009**, *42*, 1881.
(10) Concepcion, J. J.; Jurss, J. W.; Brennaman, M. K.; Hoertz, P. G.; Patrocinio, A. O. T.; Murakami Iha, N. Y.; Templeton, J. L.; Meyer, T. J. *Acc. Chem. Res.* **2009**, *42*, 1954.
(11) Nocera, D. G. *Inorg. Chem.* **2009**, *48*, 10001.
(12) Kanan, M. W.; Nocera, D. G. *Science* **2008**, *321*, 1072.
(13) Surendranath, Y.; Dinca, M.; Nocera, D. G. *J. Am. Chem. Soc.* **2009**, *131*, 2615.
(14) Lutterman, D. A.; Surendranath, Y.; Nocera, D. G. *J. Am. Chem. Soc.* **2009**, *131*, 3838.
(15) Dincă, M.; Surendranath, Y.; Nocera, D. G. *Proc. Natl. Acad. Sci. U.S.A.* **2010**, *107*, 10337.
(16) Bediako, D. K.; Lassalle, B.; Surendranath, Y.; Yano, J.; Yachandra, V. K.; Nocera, D. G. *J. Am. Chem. Soc.* **2012**, *134*, 6801.
(17) Esswein, A. J.; Surendranath, Y.; Reece, S. R.; Nocera, D. G. *Energy Environ. Sci.* **2011**, *4*, 499.
(18) Risch, M.; Khare, V.; Zaharieva; Gerencser, L.; Chernev, P.; Dau, H. *J. Am. Chem. Soc.* **2009**, *131*, 6936.
(19) Kanan, M. W.; Yano, J.; Surendranath, Y.; Dincă, M.; Yachandra, V. K.; Nocera, D. G. *J. Am. Chem. Soc.* **2010**, *132*, 13692.
(20) Risch, M.; Klingan, K.; Ringleb, F.; Chernev, P.; Zaharieva, I.; Fischer, A.; Dau, H. *ChemSusChem* **2012**, *5*, 542.
(21) Du, P.; Kokhan, O.; Chapman, K. W.; Chupas, P. J.; Tiede, D. M. *J. Am. Chem. Soc.* **2012**, *134*, 11096.
(22) Egami, T.; Billinge, S. J. L. *Underneath the Bragg-Peaks: Structural Analysis of Complex Materials*; Plenum: Oxford, 2003.
(23) Billinge, S. J. L.; Kanatzidis, M. G. *Chem. Commun.* **2004**, 749.
(24) Blakemore, J. D.; Mara, M. W.; Kushner-Lenhoff, M. N.; Schley, N. D.; Konezny, S. J.; Rivalta, I.; Negre, C. F. A.; Snoeberger, R. C.; Kokhan, O.; Huang, J.; Stickrath, A.; Tran, L. A.; Parr, M. L.; Chen, L. X.; Tiede, D. M.; Batista, V. S.; Crabtree, R. H.; Brudvig, G. W. *Inorg. Chem.* **2013**, *52*, 1860.
(25) Surendranath, Y.; Lutterman, D. A.; Liu, Y.; Nocera, D. G. *J. Am. Chem. Soc.* **2012**, *134*, 6326.
(26) Amatucci, G. G.; Tarascon, J. M.; Larcher, D.; Klein, L. C. *Solid State Ionics* **1996**, *84*, 169.
(27) Chupas, P. J.; Qiu, X.; Hanson, J. C.; Lee, P. L.; Grey, C. P.; Billinge, S. J. L. *J. Appl. Crystallogr.* **2003**, *36*, 1342.
(28) Hammersley, A. P.; Svenson, S. O.; Hanfland, M.; Hauserman, D. *High Pressure Res.* **1996**, *14*, 235.
(29) Juhas, P.; Davis, T.; Farrow, C. L.; Billinge, S. J. L., arXiv:1211.7126, arXiv.org e-Print archive, 2012; http://arxiv.org/abs/1211.7126 (accessed January 25, 2013).
(30) Delaplane, R. G.; Ibers, J. A.; Ferraro, J. R.; Rush, J. J. *J. Chem. Phys.* **1969**, *50*, 1920.
(31) Farrow, C. L.; Juhás, P.; Liu, J.; Bryndin, D.; Božin, E. S.; Bloch, J.; Proffen, T.; Billinge, S. J. L. *J. Phys: Condens. Mat.* **2007**, *19*, 335219.
(32) Masadeh, A. S.; Božin, E. S.; Farrow, C. L.; Paglia, G.; Juhás, P.; Karkamkar, A.; Kanatzidis, M. G.; Billinge, S. J. L. *Phys. Rev. B* **2007**, *76*, 115413.
(33) Petkov, V.; DiFrancesco, R. G.; Billinge, S. J. L.; Acharya, M.; Foley, H. C. *Philos. Mag. B* **1999**, *79*, 1519.
(34) Farrow, C. L.; Billinge, S. J. L. *Acta Crystallogr. A* **2009**, *65*, 232.
(35) Symes, M. D.; Surendranath, Y.; Lutterman, D. A.; Nocera, D. G. *J. Am. Chem. Soc.* **2011**, *133*, 5174.
(36) Buttry, D. A.; Anson, F. C. *Electroanal. Chem.* **1981**, *130*, 333.
(37) Blaunch, D. N.; Saveant, J. M. *J. Am. Chem. Soc.* **1992**, *114*, 3323.
(38) Hicks, J. F.; Zamborini, F. P.; Osisek, A.; Murray, R. W. *J. Am. Chem. Soc.* **2001**, *123*, 7048.
(39) Harley, S. J.; Mason, H. E.; McAlpin, J. G.; Britt, R. D.; Casey, W. H. *Chem.—Eur. J.* **2012**, *18*, 10476.
(40) Tarasevich, M. R.; Efremov, B. N. In *Electrodes of Conductive Metal Oxides, Part A*; Trasatti, S., Ed.; Elsevier: Amsterdam, 1980; Ch. 5.
(41) Trasatti, S. In *Electrochemistry of Novel Materials*; Lipkowski, J., Ross, P. N., Eds.; VCH: New York, 1994; Ch. 5.
(42) Surendranath, Y.; Kanan, M. W.; Nocera, D. G. *J. Am. Chem. Soc.* **2010**, *132*, 16501.
(43) Gerken, J. B.; McAlpin, J. G.; Chen, J. Y. C.; Rigsby, M. L.; Casey, W. H.; Britt, R. D.; Stahl, S. S. *J. Am. Chem. Soc.* **2011**, *133*, 14431.
(44) Lee, S. W.; Carlton, C.; Risch, M.; Surendranath, Y.; Chen, S.; Furutsuki, S.; Yamada, A.; Nocera, D. G.; Shao-Horn, Y. *J. Am. Chem. Soc.* **2012**, *134*, 16959.